Stochastic-dynamic analyses of subscale processes
- Observations in the tropics and applications in a GCM -

Klaus Fraedrich

Meteorologisches Institut, Universität Hamburg, Hamburg, Germany

Summary

Three stochastic-dynamic analyses of subscale processes and their effect on larger space-time scales are presented: (i) Variability induced by tropical convection scales in time as $1/f$- or flicker noise, which is related to pulse-like events. (ii) Design and analysis of a numerical experiment with a global circulation model (GCM) provides quantitative subscale statistics for parameterisation purposes. (iii) The effect of subscale forcing on the large scale circulation is demonstrated by GCM experiments with additive noise; it shows how noise can create order (coherence resonance) in complex deterministic dynamics. Introduction and outlook embed these studies between past and future.

1.   Introduction: Studies of the past

Subscale processes, their impact on atmospheric variability and parameterization are a central issue of meteorological research, both in observations, modelling, and theory. The relevance for short-term predictability and long-range variability cannot be overestimated. However, stochastic and stochastic-dynamic approaches of parameterisation of subscale processes have been confined mainly to climate research and were not prominent in numerical weather prediction. Therefore, a brief (and biased) introductory review is given first to show some earlier attempts - say twenty to thirty years ago - to stimulate research towards a direction this workshop is aiming at, namely, how to represent sub-grid processes by stochastic-dynamical models. As usual, research guidance for such studies is provided by observations and/or theoretical-dynamical analyses, while statistical-dynamical implications emerge from analytical or numerical applications.

A treatment of stochastic parameterisation may look as follows. Step-1 (*clouds as a stochastic process*): Add noise to a simple cloud model to create cloud ensemble statistics in agreement with observations. Step-2 (*clouds parameterized statistically*): Use this type of cloud statistics (supported by high resolution models or observations) to determine subscale induced ensemble sources of latent and sensible heat (and vorticity). Step-3 (*clouds organized in large scale model*): Introduce the cloud ensemble into a large scale system and evaluate the effects. If clouds are organized, say, propagating systematically different from the large scale system, the parameterisation has to be adequate. Examples of these three steps are briefly introduced before more recent issues are presented, following the same strategy.

(i) Clouds as a stochastic process: Observations of an almost log-normal distribution of cloud top heights in the tropics (Lopez 1977) initiated a stochastic view on clouds (Fraedrich 1985), to model this probability distribution and to provide the background for a stochastic cloud ensemble parameterisation scheme. Here clouds are considered as entraining jets (deterministic part), while lateral entrainment is derived as a mean plus a noisy eddy contribution. This leads to a cloud process represented by the Langevin equation,

$$dh/dz = \lambda(h_E - h) + n$$

with height z above cloud base, mean lateral entrainment rate λ, moist static energy (or any other conserved quantity) of environment h_E and cloud h, and Gaussian noise n, which represents the eddy-entrainment; $H(z)$

is the solution for $n = 0$. Defining the cloud top as the height z^* where $h_{E}(z^*) = h(z^*)$, then the first passage problem of h to reach h_E, leads to the height distribution of clouds. This is simply obtained by solving the Fokker-Planck equation for the probability density $p(h,z)$ of the cloud moist static energy evolving with height (subscripts denote differentiation):

$$p_z + \left(\lambda(h_E - h)p \right)_h - \tfrac{1}{2} B p_{hh} = 0$$

The solution, $p(h,z) = (2\pi K)^{-1/2} \exp\left[-(h - H)^2 / 2K \right]$, depends on the cloud-scale moist static energy $H(z)$ (that is, the entraining jet with zero noise, $n = 0$ and writing $h = H$) and the variance $K = <(h - H)^2> = \tfrac{1}{2} B / \lambda \left[1 - \exp(-2\lambda z)\right]$. The white noise fluctuations are vertically independent (uncorrelated) and formally derived as sub-cloud scale entrainment, $< n(z)n(z + z') >= B\delta(z')$; noise intensity $B \sim 2\sigma^2/R$ is determined by variability and average size (radius R) of the subscale thermals mixing into the plume. Now the distribution of cloud top heights can be derived, which reduces to a first passage problem for reaching an absorbing barrier at cloud top z^*, where cloud and environmental moist static energy, $h_E(z^*) = h(z^*)$, equilibrate. As the probability of $h_E(z^*) < h(z^*) < \infty$ defines the cloud top height distribution function,

$$\text{prob}(z^* > z) = P(h_0, h, z^*) = \int_{h(z^*)}^{\infty} p(h_0, h, z)dh$$

its associated density is $g(z^*|h_0, h) = -P_z$. For a parabolic h_E-profile, $h_E = h_1 + h_2 z + h_3 z^2 + ...$, analytic solutions (with B- and λ-sensitivities) are shown in Figure 1. Not unexpected, a bimodal cloud top height distribution can occur, which captures both deep convection, with an almost log-normal profile, and shallow convection, with an almost exponential structure.
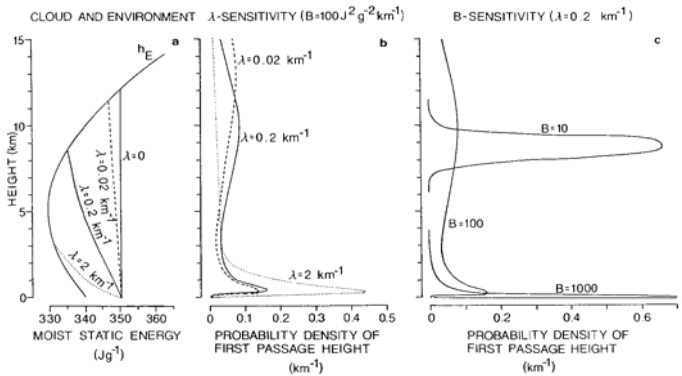

Figure 1 (a) Moist static energy of clouds with varying entrainment rates in a tropical environment h_E (above cloud base). Probability densities of first passage heights (or cloud top z^*) depending (b) on the entrainment rate (λ-sensitivity), (c) on the intensity of stochastic fluctuations (B-sensitivity).

(ii) Clouds parameterized statistically: Given such (or another) cloud top distribution, stochastic cloud ensemble parameterisations are derived. Early subscale (cloud population) statistics associated with the parameterisation problem were guided or supported by direct observations and/or high resolution model experiments (see Plank 1969, Cho 1978, Fraedrich 1977, 1978, and Beniston and Sommeria 1981, respectively). It is the cloud statistic which enters as the core ingredient of the parameterisation (just like cellular automata dynamics for organized convection). For example: Take a shallow cloud population with an exponential number density distribution (see Figure 1) of cloud tops z^* defined by the parameters K and b (as shown by Beniston and Sommeria 1981, and used by Fraedrich 1977, 1978 for cloud radius):

$g(z^*) = K\exp(-bz^*)$

Assume, based on observations and the same numerical experiments, that (i) plumes (or clouds) are 'square', $z^* = aR$, that (ii) their mass flux convergence is proportional to the mass flux m, $m_z = \lambda m$, that the entrainment rate, $\lambda = 3\alpha/R$, is inversely proportional to the radius R, etc.. Then the total number $N_0 = K/b$, area $A_0 = 2\pi N_0 K/(ab)^3$ and cloud base mass flux $M_0 = cK$ of all clouds in the population can be derived and the sources of heat, moisture and vorticity, which the subscale cloud population feeds into the large scale, can be deduced (Figure 2).
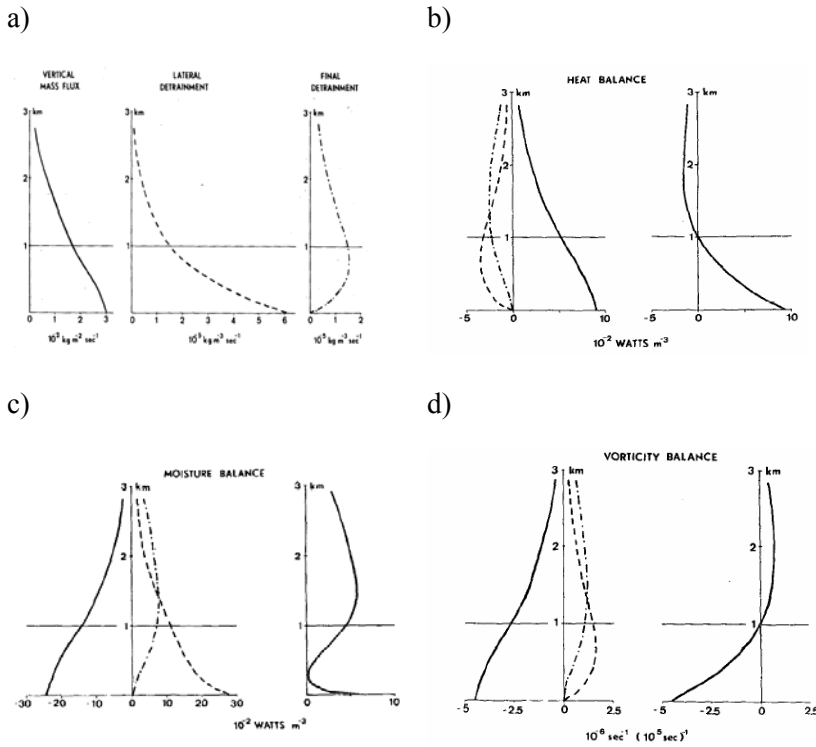
a)
b)

c)
d)

Figure 2 Mass, heat, moisture, and vorticity budget (a-d) of the cloud ensemble induced by compensating subsidence, lateral, final detrainment (full, dashed, dash dotted profile), total in right panel.

A closure is suggested linking distribution parameters (but not the statistics) with large scale dynamics by maximizing the entropy production (Fraedrich 1978). For another closure one may follow Zhang's (2002) description, who noted that 'changes in tropical tropospheric mean temperature are minuscule compared to other fields such as diabatic latent heat release and boundary layer equivalent potential temperature in tropical weather …. such observational facts are seldom considered in relation to convective parameterization in general and quasi-equilibrium in particular. The only exception is the work by Fraedrich and McBride (1989) in a theoretical study to understand the physical mechanism of CISK. They parameterized convective heating by assuming a balance between diabatic heating and adiabatic cooling in the free troposphere above the boundary layer such that the net tropospheric temperature change is zero in their two-layer model (the so called 'free ride' for convection). With this assumption .... the growth rate of CISK perturbation is independent of the horizontal scale as long as the scale of the disturbance is much smaller than the Rossby deformation radius. This resolved the long-standing problem that perturbations of smallest horizontal scales grow the fastest in classic CISK theory and offered new insight into the physical mechanism of CISK.' In this sense, the 'free ride' hypothesis may be an alternative closure.

(iii) Clouds organised in a large scale model: Organized convection effects large scale dynamical models in a different manner. This approach emerges from (i) the observation that tropical deep convection propagates westward within eastward travelling cloud clusters (Nakazawa 1988) and (ii) the CISK versus WISHE views: large scale low level cloud forcing is linked to maxima of upward motion versus zonal wind, that is, there is a phase difference in the forcing. Thus, Cho et al. (1993) present a novel view on the large scale

Madden-Julian oscillation when incorporating the effect that clouds in the Kelvin wave are organized in meso-scale clusters propagating westward with phase speed *C*. Since the phase-lag depends on the propagation speed of the Kelvin waves, they become dispersive and grow favourably at long wave lengths (see below). This study concludes that the presence of organized mesoscale cloud clusters needs to be parameterized directly into those climate models which cannot adequately describe their dynamics.

The effect of organized clouds on Kelvin waves in a shallow water equatorial beta-plane can be demonstrated by the equations of motion, thermal energy, continuity

$$u_t + \Phi_x = 0, \qquad \Phi_y + \beta u y = 0, \qquad \Phi_{pt} + S\omega = Q, \qquad u_x + \omega_p = 0$$

and hydrostasy $\Phi_p = -RT/p$ with the common notations for the zonal, meridional and vertical wind u, v, ω in *p*-coordinates, the geopotential Φ, static stability S, and heating Q. The Ansatz $\exp(i[<t + kx])$ and the trapped Kelvin wave condition, $\Phi = \Phi_0\exp(-\frac{1}{2}\beta y^2/\upsilon)$, with phase speed $c = \upsilon/k$, whose real part must be positive, yield the vertical structure equation

$$\omega_{pp} + \omega S/c^2 = Q/c^2$$

which presents an eigenvalue problem for the vertical p-velocity, $\omega(p)$. For simplicity, the heating, $Q = aS\omega^*f(p)$, with intensity a and a normalized vertical sine-profile, $f(p) = \frac{1}{2}\pi \sin(\pi(p_s - p)/\Delta p)$. The solution is

$$\omega = \frac{1}{2}a\omega^*\pi S\sin\left(\pi(p_s - p)\Delta p\right)/\left[S - (c\pi/\Delta p)^2\right]$$

The large scale condition (closure), $\omega(p^*) = \omega^*$, defines the level (say $p^* = 900$ hPa), whose vertical motion quantifies the heating Q, which gives the eigenvalue (Kelvin wave phase speed) c:

$$c = \pm\Delta p S^{1/2}/\pi\left[1 - \frac{1}{2}\pi a \sin\left(\pi(p_s - p^*)/\Delta p\right)\right]^{1/2}$$

The role of the phase difference between wave induced low-level convergence and heating localization is examined by letting the intensity depend on the phase ϕ,

$$a = a_0 \exp(i\phi) \text{ with } \phi = \frac{1}{2}\tau(C - c_r)k$$

where C is the travel-speed of the cloud clusters, their life time is τ; c_r and k are the real part of the Kelvin wave phase speed and its wave number. A half-life time of the cloud clusters of 24h (48h) and their propagation $C = -10$ ms^{-1} reveal wave number dependent growth rates, which are shown in Figure 3 (labels 1 to 3 indicate the heating intensity, $a_0 = 1.0, 2.0, 3.0$). Maximum growth rates occur in the long wave length end; there is no growth for waves shorter than wave number $k = 4$. These results suggest that organized mesoscale cloud clusters need to be parameterized directly in those climate models that cannot adequately describe their dynamics.
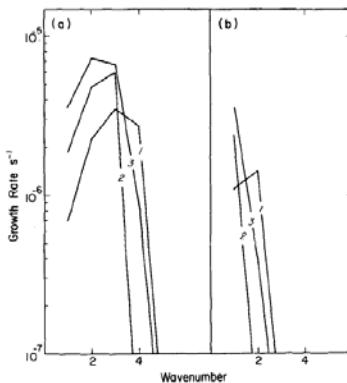

Figure 3 Growth rates of Kelvin waves when a sine heating profile is used. A phase angle between heating and wave convergence is introduced, $\phi = \frac{1}{2}\tau(C - c_r)k$, due to cloud cluster life time and propagation, τ and C. The results shown are cases with clusters propagating eastward with C = -10.0 m s^{-1}. The cluster life times are τ = 24 (a) and 48 hours (b). Labels refer to intensities a_0 = 1, 2, 3.

Outlook: These three steps provide the leitmotif for the following stochastic-dynamic studies of subscale processes and their effect on larger space-time scales: Section 2 shows that variability induced by tropical convection scales in time as 1/*f*- or flicker noise (and not in space as log-normal), which is related to pulse-like events. This result may challenge the development of subscale stochastic-dynamical models. Section 3 shows design and analysis of a numerical experiment with a global circulation model (and not a convective boundary layer model or observations) to quantify the subscale statistics for parameterisation purposes. Finally, Section 4 presents the effect of subscale forcing on the large scale circulation; here we use a GCM with additive noise (and not a linear shallow water atmosphere with organized convection), to show how noise can create order in deterministic dynamics.

2. Variability observed in the tropics: 1/f-noise and pulses

Observations give evidence that the power spectrum of tropical convective variability scales like 1/*f*-noise (with f being the frequency) within the one to thirty day period. This is first demonstrated by time series analysis of convective available potential energy, which measures the degree of convective instability, boundary layer moisture, temperature and wind speed in the tropical western Pacific (from four month TOGA-COARE). Causes and consequences are discussed (Yano et al. 2001, 2004). In this sense we follow step-1 (Introduction) aiming at the stochastic processes underlying the cloud induced variability.

1/f-noise and long-term memory: Time variability is conveniently represented by a power spectrum. If the spectrum follows a power law scaling, $S(f) \sim f^{-b}$, long-term memory can be inferred in the exponent range $0 < b < 1$, which characterizes stationary time series between white and flicker noise; larger exponents represent non-stationary processes. Flicker or 1/*f*-noise ($b = 1$) is unique in the sense that it contains equal variability for all time scales without scale separation; it is associated with intermittency and self-organized criticality.

Data analysis in the tropics: On short time scales, tropical surface conditions may be viewed as alternating between a more quiet or passive phase (of a cloud-topped fair weather boundary layer) and a pulse-like convectively active event (with drying and cooling of the boundary layer due to downdraughts) embedded in the passive phase. Thus we analyse the surface variables in two steps to determine power-law power spectra for boundary layer (temperature, mixing ratio, Figure 4; wind speed and rain rate not shown) and free atmosphere observables (CAPE): For the original time series, for time series composed of convective pulses of given length extracted by wavelets analysis, and extending this to other time series of different pulse duration.

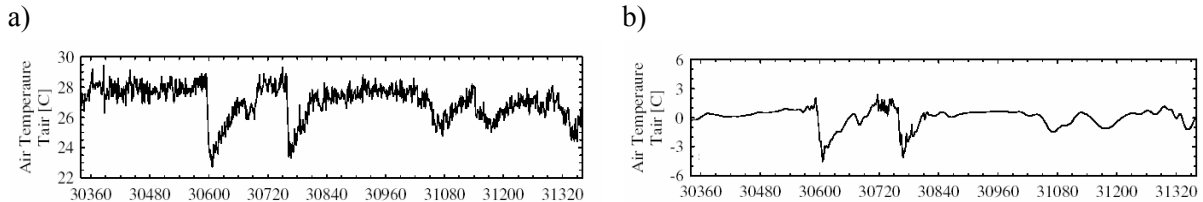a)   b)

Figure 4 A time series segment of the near surface air temperature measurements at Research Vessel Kexue, showing few cumulus convection events: (a) Pulse-like dips around t = 30 600 and 30 750 min without (a) and with (b) pulse extraction (see text).

Power spectra of the surface variables (temperature and moisture, Figure 5) reveal a 1/*f*-spectrum slope from the 1-hour scale (minimum period between 0.5 to 5 hours) extending to the intra-seasonal (30 to 60 day) time scale; likewise for CAPE which, however, due to 6 hourly resolution, spans the 1 to 30 day range.

Precipitation being closer to white noise is explained by it, rarely falling continuously into the same rain-gauge.
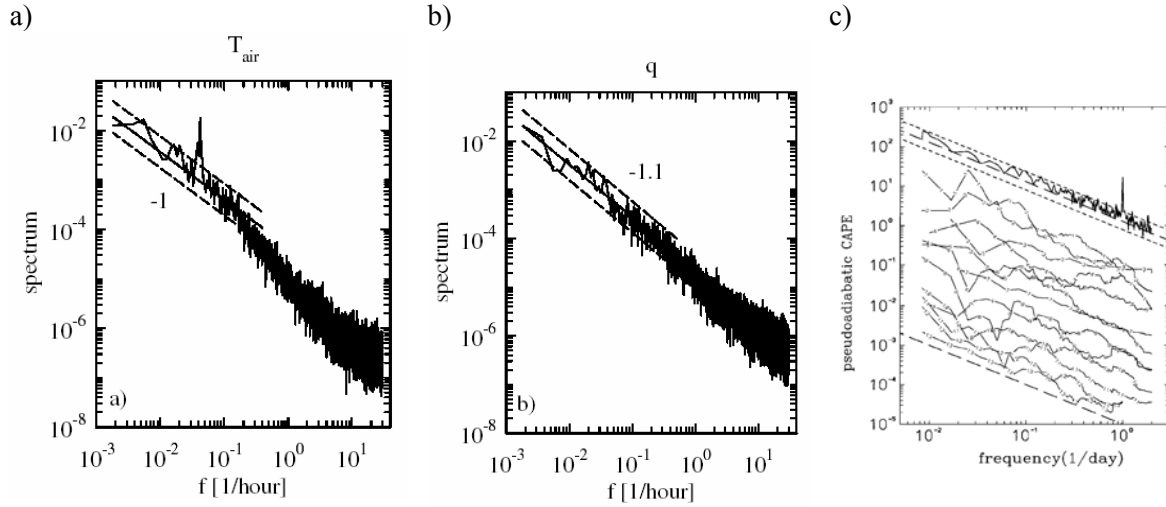
a)

b)

c)

Figure 5 Power spectra of surface measurements at research vessel 'Shiyan' for (a) air temperature, (b) moisture mixing ratio, and (c) convective available potential energy (CAPE), where f is the frequency. A 95% confidence interval is indicated (short-dashed), assuming a chi-squared distribution of errors.

Pulse extraction from time series consists of fours steps: Transform the time series to the wavelet (WL) space (using the Meyer wavelet); identify local maxima: cores of pulses; agglomerate high adjacent WL coefficients, that is, neighbours of all WLs, which exceed one standard deviation of the whole wavelet domain; reconstruct the time series comprised of signals of these single pulses (Figure 4b). The reconstructed time-series consists of pulse-like downdraught events, say of 0.5 to 5 hours duration. The power spectra of the reconstructed time series show power laws, which extend over much wider ranges than the durations of the pulse-like events, that is, almost one decade of the lower frequency and further to higher frequencies. This wide spectrum is possible as the wavelet modes extend well beyond the duration range specified for extraction. Note that the resulting spectra are close to the original and follow $1/f$-noise for periods from 1 to 10 hours (Figure 6). Repeating the procedure for 32-128 hours pulse-like events, the power law extends to the full range with slightly steeper slopes. Extension to longer time scales for the zonal wind stress observations at the equator (with 7 years hourly data based on 6 min recordings) follows approximately a $1/f$-spectrum for the range of 10 to 500 day periods, with some periodicities being embedded (Figure 6c). The zonal wind follows the same behaviour.

Further analysis shows that the pulse-like events reveal no lag-correlation for the duration of one event to the next. That is, individual pulses appear to occur as a Poisson process without mutual correlation. This excludes a $1/f$-model, which requires intervals between successive events to be highly correlated. Instead, by lack of correlation, we conclude that the total spectrum (of extracted pulse-like events) can be reproduced by a sum of spectra of individual pulse-like events and they form $1/f$-spectra for a range larger than their life-time.
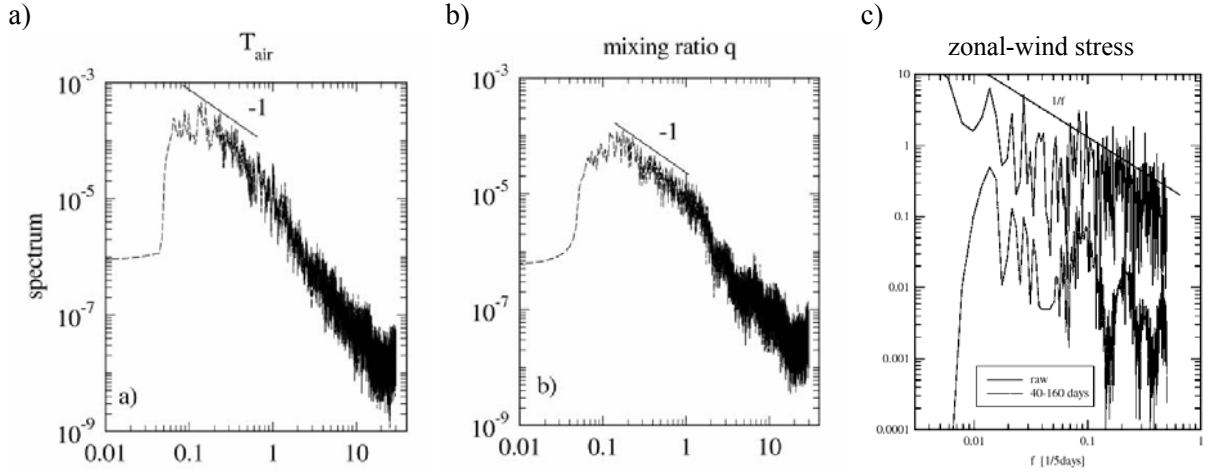
a)

b)

c)

Figure 6 Same as Figure 5, but after extraction of pulse-like events of 0.5-4 hours duration.

Conclusions: The origin and range of the $1/f$-noise in the tropical boundary layer is closely linked to pulse-like events of high intermittency: cumulus convection with downdraughts, westerly wind bursts of the Madden-Julian oscillation, and possibly ENSO. This scaling behaviour poses a challenge to the convective quasi-equilibrium hypothesis, which postulates that cumulus convection responses to large scale forcing in much shorter time than the latter so that convection is almost in equilibrium with the large scale. If this hypothesis is indeed physically valid, such a short response time must be observationally detectable. But tropical convective variability decreases at a constant rate with time scale increasing as $1/f$-noise. This scaling range extends from one hour to beyond ten days for convective and, up to several years, for surface wind stress. We propose this as an alternative view of the convective subscale processes and in support of stochastically based parameterizations. It appears that, on longer time scales (decades to millennia), sea surface temperature variability in the high-latitude North Atlantic reveals $1/f$-scaling as observed in instrumental records and coupled AO-GCM simulations (Fraedrich and Blender 2003); its origin can be related to the deep-ocean diffusion processes (Fraedrich et al. 2004).

3. Subscale forcing determined by a GCM experiment

A global atmospheric circulation model is used to derive the properties of the subscale forcing in the primitive equations (Seiffert et al. 2005). The study is based on a simulation with the model PUMA (Portable University Model of the Atmosphere, download from www.mi.uni-hh/puma), which is subject to linear diabatic heating and friction. The subscale forcing is determined for a low wave number resolution T21 (~5°x5°) embedded in T42-resolution (~ 2.5°x2.5°) using the differences between the low wave number projection of the T42-model and the forcing by low wave numbers (T21). The mean subscale forcing vanishes (besides a small heating contribution). The variance has largest values in the mid-latitudes for vorticity (mid-troposphere), temperature (lower troposphere), and in the polar mid-troposphere for divergence. The temporal correlations reveal a slow decay in the first few hours followed by an exponential decay with an e-folding time of about one day. The correlation with hyperdiffusion ($\sim[l(l+1)]^4$) is below 0.4. Based on these results the design of stochastic parameterisations is suggested.

GCM experiment (and analysis): Properties of the subscale forcing are derived by a primitive equations GCM to provide dynamical guidance for stochastic parameterisation of the unresolved subscale generated tendencies. This is useful for low resolution GCM-versions to attain climate and variability similar to the higher resolution ones. In symbolic writing non-linear (NLIN) and linear terms (LIN) are distinguished with

regard to high-resolution (subscript A for all), which is a projection to all wave numbers. L is a projection to low wave numbers (subscript L), which the pure large scale model contains.

AIM   T21-projection of T42-model = T21-model + stoch. forcing $\boldsymbol{R}$

IDEA   T42-model   (1h steps) $d\boldsymbol{X_A}/d\boldsymbol{t} = \mathrm{NLIN_A}(X_A) + \mathrm{LIN}(X_A)$

T21-projection of T42 $d\boldsymbol{X_L}/d\boldsymbol{t}|_{\mathrm{proj}} = \mathrm{NLIN_L}(X_A) + \mathrm{LIN}(X_L)$

T21-model $d\boldsymbol{X_L}/d\boldsymbol{t}|_{\mathrm{T21}} = \mathrm{NLIN_L}(X_L) + \mathrm{LIN}(X_L)$

| Residual tendency (difference) $\boldsymbol{R} = \mathrm{NLIN_L}(X_A) - \mathrm{NLIN_L}(X_L)$ |

Thus the difference of the two large scale tendencies with regard to T21 characterizes the subscale forcing (residual tendencies), one is obtained by projection from all T42 interactions, the other from T21 interactions. All tendencies can be computed on a term to term basis (schematic example: hyperdiffusion, Figure 7).
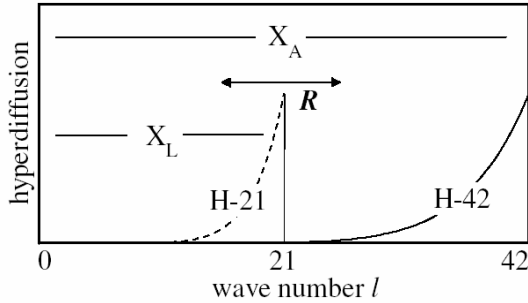

Figure 7 Schematic scale separation for all (X_A) and large scale variables (X_L) in wave number space. $\boldsymbol{R}$ denotes the residual tendencies with upward and downward fluxes across the cut-off scale '21'. The curves show relative magnitudes of hyperdiffusion ($\sim [l(l + 1)]^4$) for the high resolution (H-42, solid) and the low resolution (H-21, dashed).

The main properties (shown only for the vorticity equation, Figure 8) are as follows:

- The residuals have zero mean besides a small temperature forcing which explains the higher global mean temperature in the high resolution model.

- The variability of the residuals is concentrated in the high total wave number range.

- The vorticity and divergence residuals are concentrated in the mid-troposphere whereas temperature is mainly forced in the lowest model level.

- The probability distribution of the residuals is predominantly Gaussian, but shows exponential tails for vorticity and temperature.

- The decorrelation time is of the order of one day, below 6 hours the residuals remain approximately constant.

- The correlation between vertical levels is largest for the vorticity and the divergence in the mid-troposphere, but weak for the temperature.

- The correlations between the residuals and the variables are slightly negative and hint to damping time scales of 20 days for vorticity, 40 days for temperature and 2 days for divergence.

- A minor part of the residuals can be considered as hyperdiffusion (correlation up to 0.4); for vorticity in the whole troposphere, for temperature and divergence only in the lowest level.
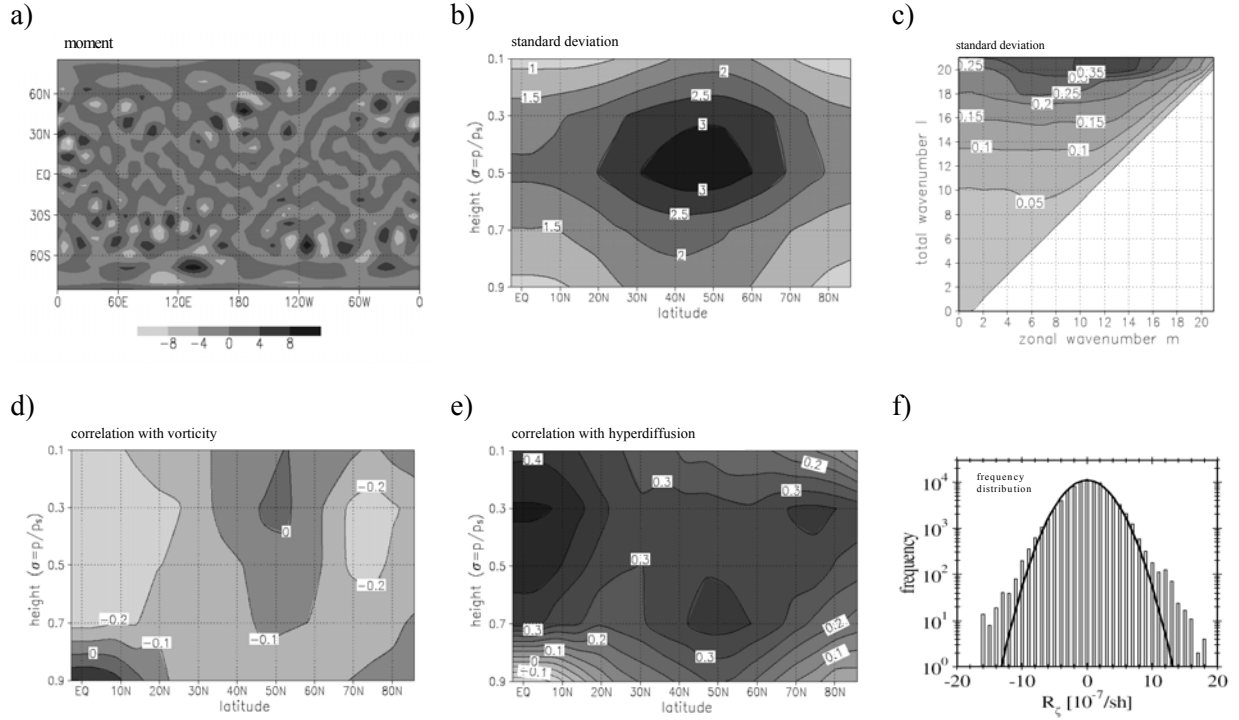
Figure 8 Residuals of the vorticity [10^{-7}/sh]: (a) Snapshot in the mid-troposphere, (b) standard deviation in latitude-height cross-section, (c) standard deviation in total, l, and zonal wave number, m, domain, (d) correlation with the vorticity in latitude-height cross-section, (e) correlation with vorticity hyperdiffusion in latitude-height cross-section, (f) frequency distribution of a time series in the mid-troposphere 47N.

Conclusion: These results subsume main statistical properties of the residual tendencies to be used in stochastic parameterisations. The properties above serve as a guide to design the stochastic forcing of a low resolution T21-model. A first hint is the concise structure of the residuals. They are dominant in the high total wave number space and, in the vertical, at different heights for each model variable, vorticity, temperature, and divergence. Vertical correlations show weak values for vorticity and divergence, whereas the temperature forcing is uncorrelated. The temporal behaviour can be reproduced by an autoregressive process of first order with the decay time of one day. A possible extension of the present study pertains to the downscale energy flux and hyperdiffusion. Although the correlation of the residuals with hyperdiffusion is low (below 0.4), this parameterisation, which is common in many atmospheric models, could be improved using the present results. Preliminary investigations show that in a pure dynamical model the effects of stochastic parameterisation based on the major results above are relatively small. However, future applications of these results aim at stochastic parameterisation in fully parameterised models of intermediate complexity (MICs, Fraedrich et al. 2005a,b; www.mi.uni-hamburg.plasim). Stochastic forcing is expected to improve climate simulations since, in particular, prediction of precipitation has benefited. A further useful application of the present approach is the quantification of localised forcing terms required in simple linear models of the global atmosphere.

4. Stochastic forcing of a GCM: Coherence resonance

It is not unusual that response mechanisms are disclosed by noise, which would otherwise remain obscured in purely deterministic dynamics. For example, a reduced gravity ocean basin realises spatial resonance (Sura et al. 2000, 2001), by its dynamical response on spatially inhomogeneous stochastic forcing. In an atmospheric GCM coherent resonance, which contributes to the intra-annual variability, is discovered, by which spatio-temporal regularity is enhanced due to stochastic forcing. It is shown that zonal wave number 6

disturbances in the summer hemispheric mid-latitudes become ordered by noise (Perez-Munuzuri et al. 2005).

Background: Although some of the present state-of-the-art coupled atmosphere-ocean global circulation models (albeit resorting to purely deterministic parameterizations) succeed to account for the high-frequency part of the power spectrum up to decades, the need for a stochastic ingredient in the parameterization of sub-grid processes is recognized. The main reasons are the inherent uncertainties about the proper way to account for unresolved processes, and the experimental errors. The well-known phenomenon of stochastic resonance (Benzi et al. 1981, 1982), which is a paradigm of the constructive effects of noise on nonlinear systems, can be regarded as a by-product of a recent trend in climate research, known as *stochastic parameterization*. The first attempted application of stochastic resonance was to explain within a very simple energy-balance model climatic variability at the glaciation timescale. A close relative of stochastic resonance, also known as "internal" or "autonomous" stochastic resonance, is *coherence resonance* (Pikovsky and Kurths 1997, see also Benzi and Sutera 2004) wherein noise enhances the coherence of the inherent modes of the system without the presence of periodic forcing as in stochastic resonance: for an intermediate level of noise, a peak appears in the spectral density at a given frequency. Other situations have been studied in the literature, both theoretically and experimentally, of which the most paradigmatic are *excitable systems* and *noisy precursors* of a variety of bifurcations.

GCM experiment (and analysis): In the context of atmospheric dynamics, it is the first example of the coherence resonance phenomenon, which is described here. It contributes to intra-annual variability as it appears far from the bifurcation to periodic solutions. The experiments are conducted with the Portable University Model of the Atmosphere (PUMA, available from www.mi.uni-hamburg/puma). Stochastic forcing is added to the thermodynamic equation as Gaussian noise with zero mean, delta correlated in space and time, and with different intensities A, varying from 10^{-7} via 4.10^{-5} to 4.10^{-3} (the units correspond to K/day heating rates). The 300hPa vorticity field (Figure 9) is a snapshot representative for a permanent summer in the aqua-planet's northern hemisphere (60K north-south pole temperature difference).
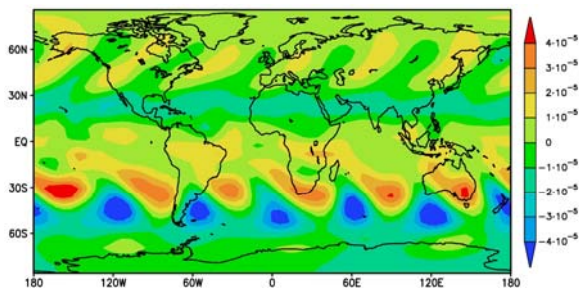

Figure 9 Vorticity field (snapshot) of 300 hPa for the reference temperature difference of 60K between the poles (permanent summer in the northern hemisphere).

Figure 10 depicts the time evolution of vorticity and its corresponding power spectrum at a given grid point 47° N, 0° E, in the case of Figure 9 and for three different noise amplitudes. Time series and power spectra clearly demonstrate the effect of coherence resonance when increasing the noise intensity A. For the intermediate value $A = 4.10^{-5}$, the series appears more regular, which is confirmed by the power spectrum narrowest and highest peak. For very low values of noise, the peak around the mean frequency is wider and lower. For large noise amplitudes the power spectrum becomes broadband, and intermittent regions of noisy periodic oscillations and noise-dominated regions are observed. These observations point to a resonant behaviour since the temporal evolution of the pattern becomes more regular as *A* is increased, but this regularity becomes deteriorated past some optimal value of *A*.
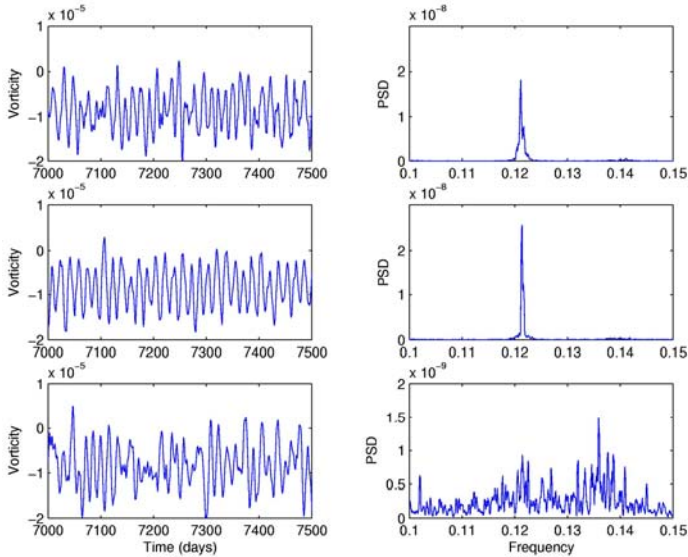
Figure 10 Vorticity time series (left) and their respective power spectra (right) in the summer hemisphere at 47° N, 0° E. From top to bottom the noise intensity increases: $A = 10^{-7}$, $A = 4.10^{-5}$, and $A = 4.10^{-3}$.

To characterize quantitatively the observed ordering, we compute as function of the noise amplitude *A*, a measure traditionally used to study coherence resonance: the *coherence factor* $\beta = H/W$, where *H* is the height and *W* the relative width of the dominant peak in the power spectrum. The higher and/or narrower the peak, the larger the temporal regularity of the vortical pattern. The following results are noted: (i) The nontrivial behaviour of β as a function of *A* is well pronounced at mid-latitudes in the summer hemisphere with a maximum at intermediate values, which means that the vorticity time series becomes more regular, as expected for coherence resonance. (ii) The effect of noise on the global circulation is more pronounced in the summer hemisphere, where the amplitude of the deterministic signal is weaker, i.e. the absolute values of are smaller than in the winter hemisphere. (iii) Both an increase in *H* and a decrease in *W* contribute to maximize the coherence for some intermediate value of noise. (iv) For high noise intensities in the summer hemisphere β goes to zero since the spectrum becomes broadband (Figure 10, bottom) leading to smaller values of *H* than of *W*. (v) For low noise intensities, β does not tend to zero (Poissonian limit) since the noiseless model exhibits a quasi-periodic behaviour. Although the vorticity time series shows a periodic behaviour for low *A*, the ratio *H/W* is smaller than for intermediate noise intensities see, for example, the spectral densities in Figure 10.
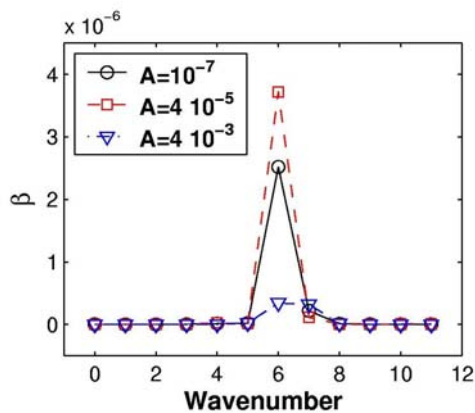

Figure 11 Coherence factor β as a function of wavenumber for three different values of the stochastic forcing intensity A. Note the resonant peak in wavenumber 6.

The effect of white noise is more relevant for mid-latitudes in the summer hemisphere, where β attains its maximum value. At these latitudes the deterministic vortical pattern is neither ordered nor strong enough to

clearly stand out above the background, although a pattern of waves with zonal wavenumber 6 circling the globe can be easily appreciated from Figure 9. Zonal wavenumber 6 (mode-6) is the dominant one in the sense that it is most responsible for the fluctuations at a grid point induced by the corresponding traveling mode-6 pattern. Figure 11 shows the contribution of each spectral mode of the vorticity field to β at the mid-latitude analyzed and for three different values of noise intensity. Note that mode-6 contributes most strongly to the enhanced regularity compared to the remaining modes and attains a maximum value for an intermediate level of noise. And thus it proves to be the mode responsible for the coherence resonance phenomenon. Adding noise to a pre-existing, nearly ordered pattern reinforces the resonance. On the other hand, for the winter hemisphere (independently of latitude) vortical patterns are so well defined but noise cannot affect their behaviour. The meaning of β being different from zero in the winter hemisphere is that some oscillatory behaviour exists in the model dynamics, but no ordering i.e., a bell-shaped functional dependence on A as expected for coherence resonance and observed in the summer hemisphere occurs as noise increases.

Conclusion: The results highlight the potential of introducing noise into numerical weather prediction (NWP) models where the noise-amplitude becomes a crucial parameter. A consequence for NWP strategy is to perform forecasts with ensemble sets forced by different noise levels. In the experiments above, noise is added at each time step which, in a first approximation, is independent in space and in time. However, uncorrelated noise may be a too idealistic assumption in general. In particular, the introduction of noise correlated in space and time has significant influence on, for example, ensemble weather forecasting (Perez-Munuzuri et al. 2004). Our results suggest that noise has the ability to enhance predictability of vortical patterns in such high-dimensional systems as an atmospheric GCM by generating higher regularity. In nature, there are additional causes for the variability of vortical structures: they are influenced by orography, moist processes, etc., which are not solved by PUMA. Nevertheless, wind anomalies which originate in the tropics and propagate slowly poleward do occur in the atmosphere and tend to be much more coherent in the summer hemisphere than in the winter one. A plausible explanation for this different behaviour could be the presence of noise which, being ubiquitous in nature and in atmospheric models, makes the weaker summer hemisphere structures appear in a more regular fashion.

5.   Outlook

Three studies on subscale stochastic-dynamic processes are presented: (i) Observational experiments show that boundary layer variability in the tropics scales as $1/f$-noise, which is induced by pulse-like events of convection. For adequate stochastic subscale modelling further theoretical research is required. (ii) Design and analysis of a general circulation model experiment allow the derivation of the large scale impact of subscale processes in a systematic manner. The aim is to obtain quantitative estimates for stochastic-dynamic parameterisation. (iii) General circulation model experiments show how noise can create order in deterministic dynamics. Extension to the impact of organized stochastic subscale models (or correlated noise) is necessary. Details are available from the cited papers and those referenced there.

References

Beniston, M. G. and G. Sommeria, 1981: Use of a detailed planetary boundary layer model for parameterisation purposes. *J. Atmos. Sci.* **38**, 780-797

Benzi, R., A. Sutera, and A. Vulpiani, 1981: The mechanism of stochastic resonance. *J. Phys.* A **14**, L453-457

Benzi, R., A. Sutera, and A. Vulpiani, 1982: Stochastic resonance in climate change. *Tellus* **34A**, 10-16

Benzi, R. and A. Sutera, 2004: Stochastic resonance in two-dimensional Landau-Ginzburg equation. *J. Phys.* A: Math. Gen. 37, L391-398

Cho, H.-R. 1978: Some statistical properties of a homogeneous and stationary cumulus cloud field. *J. Atmos. Sci.* **35**, 125-138

Cho, H.-R., K. Fraedrich, and J. T. Wang, 1994: Cloud clusters, Kelvin wave-CISK and the Madden-Julian oscillation in the equatorial troposphere. *J. Atmos. Sci.* **51**, 68-76

Fraedrich, K., 1977: A mass budget of an ensemble of transient cumulus clouds determined from direct cloud observations. *J. Atmos. Sci.* **33**, 262-268

Fraedrich, K., 1978: Further studies on a transient cumulus cloud ensemble and its large scale interaction. *J. Atmos. Sci.* **34**, 335-343

Fraedrich, K., 1985: On the distribution of cloud top heights based on stochastic forcing. *Tellus* **37A**, 176-184

Fraedrich, K. and J. L. McBride, 1989: The physical mechanism of CISK and the free-ride balance. *J. Atmos. Sci.* **46**, 2642-2648

Fraedrich, K. and R. Blender, 2003, 2004: Scaling of atmosphere and ocean temperature correlations in observations and climate models. *Phys. Rev. Lett.* **90**, 108501 and *Phys. Rev. Lett.*, **92**, 039802.

Fraedrich, K., U. Luksch, and R. Blender, 2004: 1/f-model for long-time memory of the ocean surface temperature. *Phys. Rev.* E **70**, 037301

Lopez, R. E., 1977: The log-normal distribution and cumulus cloud observation. *Mon. Wea. Rev.* **105**, 865-872

Nakazawa, T., 1988: Tropical superclusters within intra-seasonal variations over the Western Pacific. *J. Meteor. Soc. Japan* **66**, 823-839

Pérez-Munuzuri, V., M. N. Lorenzo, P. Montero, K. Fraedrich, E. Kirk, and F. Lunkeit, 2004: Spatio-temporal stochastic forcing of an ensemble of global circulation models. *Nonlinear Processes Geophys.* **10**, 453-461

Pérez-Munuzuri, V., R. Deza, K. Fraedrich, T. Kunz, and F. Lunkeit, 2005: Coherence resonance in an atmospheric GCM. *Phys. Rev.* E **71**, 065602 (1-4)

Pikovsky, A. S. and J. Kurths, 1997: Coherence resonance in a noise-driven excitable system. P*hys. Rev. Lett.* **78**, 775-778

Plank, V.G., 1969: The size distribution of cumulus clouds in representative Florida populations. *J. Appl. Meteor*. **8**, 46-67

Seiffert, R, K., R. Blender, and K. Fraedrich, 2005: Subscale forcing in a global circulation model and stochastic parameterisation. *Q. J. R. Meteorol. Soc.,* submitted

Sura, P., F. Lunkeit, and K. Fraedrich, 2000: Decadal variability in a simplified wind-driven ocean model. *J. Phys. Oceanogr*. **30**, 1917-1930

Sura, P., K. Fraedrich, and F. Lunkeit, 2001: Regime transitions in a stochastically forced double-gyre model. *J. Phys. Oceanogr*. **31**, 411-426

Yano J.-I., K. Fraedrich, and R. Blender, 2001: Tropical convective variability as 1/f-noise. *J. Climate* **14**, 3608-3616

Yano J.-I., R. Blender, C. Zhang, and K. Fraedrich, 2004: 1/f-noise and pulse-like events in the tropical atmospheric surface variability. *Q. J. R.. Meteorol. Soc*. **130**, 1697-1721

Zhang, G. J., 2002: Convective quasi-equilibrium in mid-latitude continental environment and its effect on convective parameterization, *J. Geophys. Res*. **107** (D14)